ACS OMEGA

Open Access



http://pubs.acs.org/journal/acsodf

Article

# Controlling N-Doping Nature at Carbon Aerogels from Biomass for Enhanced Oxygen Reduction in Seawater Batteries

Susanto Susanto, Tantular Nurtono, Widiyastuti Widiyastuti, Min-Hsin Yeh, and Heru Setyawan*

Cite This: *ACS Omega* 2024, 9, 13994−14004

Read Online

ACCESS | Metrics & More | Article Recommendations | Supporting Information

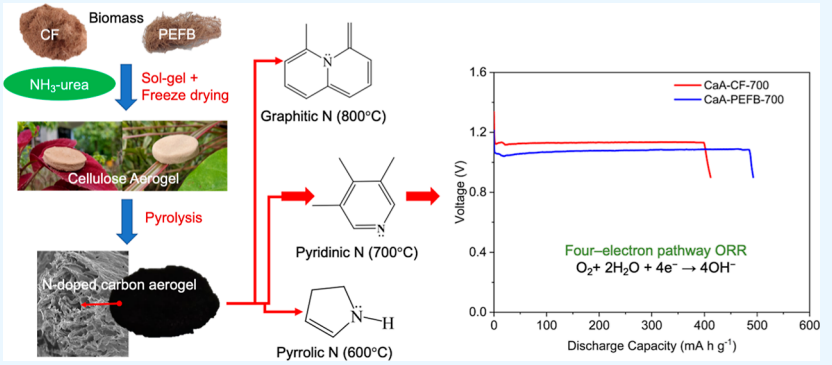


**ABSTRACT:** Pyridinic N-type doped at carbon has been known to have better electrocatalytic activity toward the oxygen reduction reaction (ORR) than the others. Herein, we proposed to prepare pyridinic N doped at carbon aerogels (CaA) derived from biomass, i.e., coir fiber (CF) and palm empty fruit bunches (PEFBs), by adjusting the pyrolysis temperature during carbonization of the biomass-based-cellulose aerogels. The cellulose aerogels were prepared by the ammonia−urea system as the cellulose solvent, in which ammonia also acted as a N source for doping and urea as the cellulose cross-linker. The as-prepared cellulose aerogels were directly pyrolyzed to produce N-doped CaA. It was found that the type of N doping is dominated by pyrrolic N at pyrolysis temperature of 600 °C, pyridinic N at 700 °C, and graphitic N at 800 °C. The pyridinic N exhibited better performance as an electrocatalyst for the ORR than pyrrolic N and graphitic N. The ORR using pyridinic N follows the four-electron pathway, which quantitatively implies a more electrochemically stable process. When used as a cathode for the Mg−air battery using a 3.5% NaCl electrolyte, the pyridinic N CaA exhibited excellent performance by giving a cell voltage of approximately 1.1 V and delivered a high discharge capacity of 411.64 mA h $g^{-1}$ for CF and 492.64 mA h $g^{-1}$ for PEFB corresponding to an energy density of 464.23 and 529.49 mW h $g^{-1}$, respectively.

## 1. INTRODUCTION

The scarcity and high cost of the lithium precursor for lithium-ion batteries (LIBs) that currently dominate the power source market of advanced consumer electronics and electric vehicles endanger the stable supply of LIBs.[1] These have encouraged many researchers to find new redox chemistries for batteries that have high energy density, safety, and low cost. Metal−air batteries (MABs) are one of the promising systems and have been investigated tremendously due to their very high theoretical energy densities, exceeding those of LIBs.[2−4] In addition, MABs can be operated using aqueous electrolytes, sustainable and abundant raw materials, that make the system intrinsically cost low, highly safe, and environmental benign.[5−8] Among the various MAB systems, seawater batteries consisting of metal anode, air cathode, and seawater electrolyte have drawn great attention because of their good electrochemical performance and the sufficiently available of seawater on earth with a relatively homogeneous geographic distribution.[9−11] One of the main obstacles in MABs is the sluggish oxygen reduction reaction (ORR) in the three-phase reaction zone of the air cathode that requires a highly active electrocatalyst hosted in a highly porous material to overcome the air diffusion resistance.[12,13] Noble-metal-based electrocatalysts are considered the benchmark electrocatalyst for the ORR, but their practical applications are hindered by their scarcity and expensive cost.[14] Therefore, it is urgent to explore new sorts of highly efficient, stable, and low-cost ORR electrocatalysts replacing the noble-metal-based ones.[15] Owing to their low cost, environment-benignity, and abundant

Received: November 21, 2023
Revised: February 21, 2024
Accepted: February 27, 2024
Published: March 14, 2024

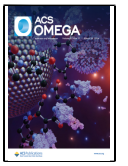

reserves, N-doped carbon materials are considered as the promising alternatives to the noble metals.[12,16]

Three types of N functional groups are generally observed in the N-doped carbon materials such as graphene, carbon nanotubes, fullerene, and graphite: pyrrolic N, pyridinic N, and graphitic N.[17,18] Among those three, pyridinic N is considered as the most efficient for the ORR, and its activity is determined by the N-doping concentration.[18−22] Carbon materials with abundant exposed edges that provide sites for N doping are desirable to enhance ORR electrocatalysis and, thus, a new type of carbon framework as the matrix for pyridinic N doping is required to be explored.[18,23] Carbon aerogel, which has a three-dimensional porous network filled with 90−99% of gas, can be an excellent candidate for such purposes. Its highly porous network confers various unique properties such as ultralow density, large specific surface area, and high electrical conductivity that make carbon aerogel suitable for electrodes for electrochemical energy storage and conversion devices.[24−26] Carbon aerogel is typically prepared by pyrolysis of a highly cross-linked polymeric gel obtained by the sol−gel process with specific drying under an inert atmosphere. The use of renewable natural-origin polymers such as cellulose and lignin as precursors can significantly reduce cost and improve sustainability.[27] Moreover, pyrolyzing N-rich natural polymers can produce N-doped carbon aerogel directly without additional nitridation process, which is typically energy intensive and time-consuming, for doping.[24,28,29]

Previously, we had successfully prepared carbon aerogels using coir fibers (CFs), an abundantly available agricultural waste rich in cellulose, as carbon precursors by direct pyrolysis of cellulose aerogel derived from the material.[12,30] To enrich cellulose aerogel with nitrogen as a source for N doping, an aqueous ammonia−urea system was used as the solvent for cellulose during the sol−gel process. This way, N-doped carbon aerogel could be obtained in situ during pyrolysis which is more straightforward and has greater potential to get high N content and stable product.[31] The N-doped carbon aerogel exhibited an excellent electrocatalytic activity toward ORR in alkaline media following a two-electron-transfer mechanism.[12] However, peroxide emerges as an intermediate in the ORR in this two-electron process, not directly converted into water without side reactions as in the four-electron-transfer process.[23] Therefore, the four-electron pathway is preferable due to the more efficient and favorable process for the ORR, and the N-doped carbon aerogel should be designed to fulfill this task.

During the carbonization process using slow pyrolysis of N-containing cellulose aerogel, temperature is a critical factor influencing the N content and the nature of N doping in carbon materials.[31] For example, the N-content of the residue carbonaceous materials decreases with increasing temperatures, and pyridinic N and pyrrolic N are cracked to produce HCN and $NH_3$ at high temperatures.[32−35] In general, the pyrolysis process of cellulosic materials involves consecutive steps including dehydration (<200 °C), volatilization (200−500 °C), and carbonization (>500 °C) by depolymerization of hemicellulose, cellulose, and lignin. Carbonization occurs with minimal weight loss as the temperature increases, but there are essential changes in the solid structure. Therefore, it was assumed that the nature of the N doping can be regulated by adjusting the pyrolysis temperature during the carbonization process.

In this work, we report on the preparation of N-doped carbon aerogels using biomass, i.e., CFs and palm empty fruit bunches (PEFB), as a carbon precursor for use as an electrocatalyst for the ORR. The ammonia−urea system is used as the cellulose solvent during the sol−gel process to enrich the N-content in cellulose aerogel to increase the content of N doped during pyrolysis. The effect of temperature on the type of N doping and the structure of the carbon aerogels produced is investigated. The electrocatalyst activity of the N-doped carbon aerogel toward the ORR is examined in a 3.5% NaCl electrolyte. Then, the N-doped carbon aerogels are assembled as a cathode of a Mg−air battery with magnesium alloy as the anode, and their performance is tested.

## 2. EXPERIMENTAL SECTION

**2.1. Materials.** CF was obtained from Tulungagung, Indonesia, and PEFBs were obtained from PT. Polytech Indonesia. The cellulose content of CF and PEFB, as determined by the Chasson−Datta method, was 39.28 and 49.36%, respectively. The proximate composition of CF was 6.73% moisture, 3.36% ash, 56.05% fixed carbon, and 33.86% volatile matter and of PEFB was 8.46, 3.86, 55.76, and 31.92%. In addition, PEFB contained an oil content of approximately 0.39%. Sodium hydroxide (NaOH; reagent grade), ethanol (99.9%; reagent grade), ammonia ($NH_3$ 25%; reagent grade), and sodium chloride (NaCl; reagent grade) were purchased from Merck. Urea [$(NH_2)_2CO$; commercial grade] was provided by PT. Petrokimia Gresik, Indonesia. Polyvinylidene fluoride (PVDF; reagent grade) and 1-methyl-2-pyrrolidinone (NMP; reagent grade) were purchased from Sigma-Aldrich. Nickel foam and magnesium alloy AZ31B sheet were used as the current collector and negative anode, respectively, during the electrochemical performance tests. Demineralized water was used for all syntheses and for preparing electrolytes for electrochemical performance tests. All chemicals were used as received without further purification.

**2.2. Preparations of N-Doped Carbon Aerogels.** N-Doped carbon aerogels were prepared from either CF or PEFB raw material following our previous method with some modifications.[12] Briefly, the raw material was first converted into cellulose aerogel and then pyrolyzed at high temperature under a nitrogen environment. To prepare the cellulose aerogel, the raw material was milled, sieved to 120 mesh (125 $\mu$m), and digested in 6% NaOH solution under atmospheric reflux for 4 h to produce pulp. For the PEFB raw material, it was first pretreated with a 4% NaOH solution to eliminate the oil content.[36] The resulting pulp was filtered, washed, and dissolved in an aqueous ammonia−urea solution consisting of 5.0 mL of water, 4.0 g of urea, and 11 mL of 25% aqueous $NH_3$ solution under ultrasonication for 30 min. Then, the mixture was cooled at a temperature of −5 °C for 24 h to allow for gelation. The gel was thawed at room temperature for 1 h, immersed in ethanol 98% for 24 h for coagulation, and soaked in water to exchange ethanol with water. The cellulose aerogel was obtained by freezing the hydrogel at −20 °C for 24 h, followed by vacuuming to 20 Pa at −40 °C in a freeze-dryer (EYELA FDU-1200) for 24 h. The cellulose aerogel was pyrolyzed in a furnace under the nitrogen atmosphere at a temperature varied from 600 to 800 °C. The pyrolysis vessel was purged with nitrogen for 15 min before heating. The heating was carried out in steps, starting from 150 °C for 30 min to remove moisture, 400 °C for 30 min to decompose



https://doi.org/10.1021/acsomega.3c09297
ACS Omega 2024, 9, 13994−14004

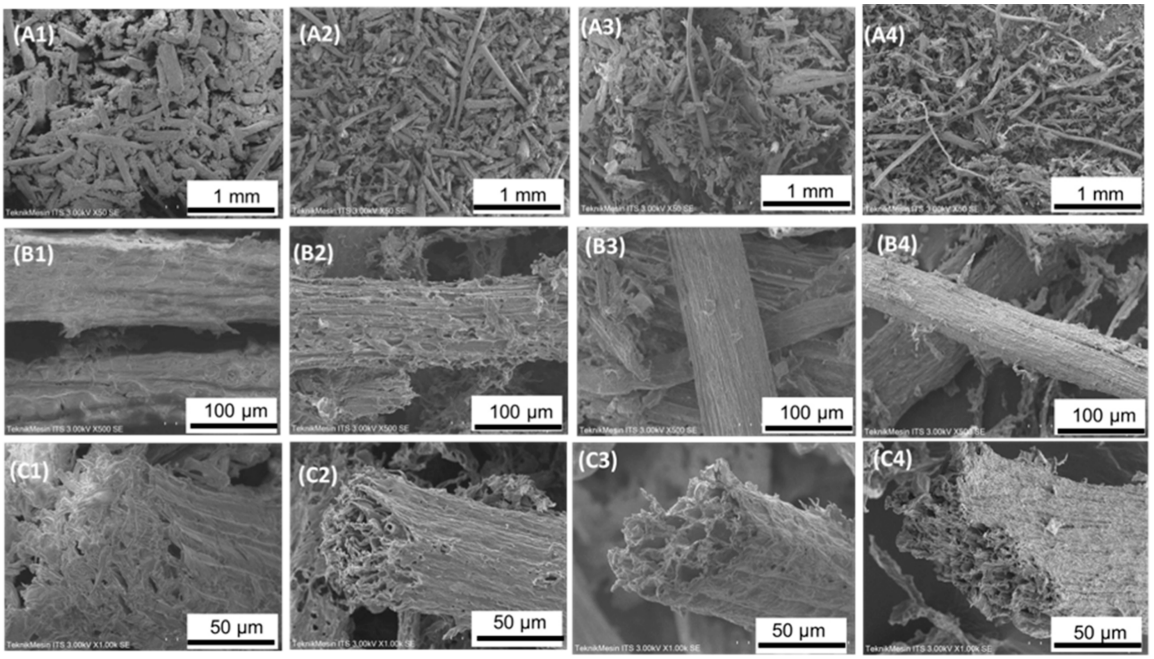


**Figure 1.** (A1−C1) Morphology of CF cellulose aerogels; (A2−C2) morphology of CF carbon aerogels (CaA) pyrolyzed at 700 °C; (A3−C3) morphology of PEFB cellulose aerogels; and (A4−C4) morphology of PEFB CaA pyrolyzed at 700 °C.

cellulose and lignin, and the pyrolysis temperature for 2 h to carbonize cellulose.

**2.3. Characterization.** The chemical functional groups of the samples were identified by Fourier transform infrared spectroscopy (FTIR; Thermo Scientific Nicolet iS10) at wavenumbers ranging from 4000 to 400 $cm^{-1}$. The morphology and atomic composition were observed by scanning electron microscopy with energy-dispersive X-ray spectroscopy (SEM−EDS; Hitachi FlexSEM 1000). The crystalline phase was identified by X-ray diffraction (XRD; PANalytical, X'pert Pro) in the $2\theta$ interval of 20−80°. The specific surface area was determined from the $N_2$ adsorption isotherms (Nova 1200, Quantachrome) using the multiple-point Brunauer−Emmett−Teller (BET) method at $P/P_0 < 0.3$. Prior to the measurement, the sample was degassed by heating at temperature of 300 °C under flowing nitrogen for 3 h. The porosity of aerogel was calculated using

$$\phi = 1 - \frac{\rho_b}{\rho_t} \tag{1}$$

where $\phi$ is the porosity, $\rho_b$ is the bulk density of aerogel obtained by measuring the mass and the bulk volume of samples, and $\rho_t$ is the true density of cellulose (=1.528 g $cm^{-3}$).[37]

**2.4. Electrochemical Performance Test of N-Doped Carbon Aerogel.** The electrocatalytic activity of the prepared N-doped carbon aerogel was studied for the ORR using cyclic voltammetry (CV) and linear sweep voltammetry (LSV) methods in a three-electrode setup. The three electrodes were connected to a potentiostat/galvanostat instrument (Autolab PGSTAT 302, Metrohm). The catalyst ink was prepared by mixing 10 mg of carbon aerogel with 1 mg of PVDF binder and 0.3 mL of NMP solvent. Then, 0.010 mL of the carbon ink was drop-casted onto a surface of 3 mm glassy carbon (geometric area = 0.071 $cm^2$) and dried at 50 °C with a catalyst loading of 0.8 mg. Pt coil and Ag/AgCl were used as the counter and the reference electrodes, respectively. All measurements were performed under ambient conditions.

The electrochemical measurements were performed in an oxygen-saturated 3.5% sodium chloride (NaCl) solution. Prior to the measurements, the NaCl solution was purged with oxygen for 30 min and maintained under an oxygen atmosphere during the electrochemical test. The CV measurement was performed by scanning the potential between −1.0 and +1.0 V (vs Ag/AgCl) at a scan rate of 10 mV $s^{-1}$. LSV was performed on a rotating disc electrode (RDE) by varying the rotation speed from 400 to 3600 rpm, and the potential was scanned from −0.7 to 0.0 V (vs Ag/AgCl) at a scan rate of 10 mV $s^{-1}$. The number of transferred electrons and the kinetics of current density were predicted using the Koutecký−Levich (K−L) equation

$$\frac{1}{i} = \frac{1}{B\omega^{1/2}} + \frac{1}{i_k} \tag{2}$$

$$B = 0.201nFC_{O_2}D_{O_2}^{2/3}\nu^{-1/6} \tag{3}$$

where $i$ is the current density (mA $cm^{-2}$), $\omega$ is the electrode rotation speed (rpm), $i_k$ is the kinetic current density (mA $cm^{-2}$), $n$ is the number of electrons involved in ORR, $F$ is the Faraday constant, $C_{O_2}$ is the saturated oxygen concentration ($9.38 \times 10^{-5}$ mol $cm^{-3}$),[38] $D_{O_2}$ is the diffusion coefficient of oxygen in the electrolyte ($2.17 \times 10^{-5}$ $cm^2$ $s^{-1}$),[39] and $\nu$ is the kinematic viscosity of the electrolyte ($8.61 \times 10^{-2}$ $cm^2$ $s^{-1}$).[38] The CV measurement was also carried out in a nitrogen-saturated 3.5% NaCl solution. In this case, prior to the measurements, the NaCl solution was purged with nitrogen to remove oxygen and maintained under a nitrogen atmosphere during the electrochemical test using conditions the same as those for an oxygen atmosphere.

The as-prepared carbon aerogels were also used as cathode materials for Mg−air seawater battery full-cell testing. First, carbon aerogel powder and PVDF binder were mixed in the


https://doi.org/10.1021/acsomega.3c09297
ACS Omega 2024, 9, 13994−14004

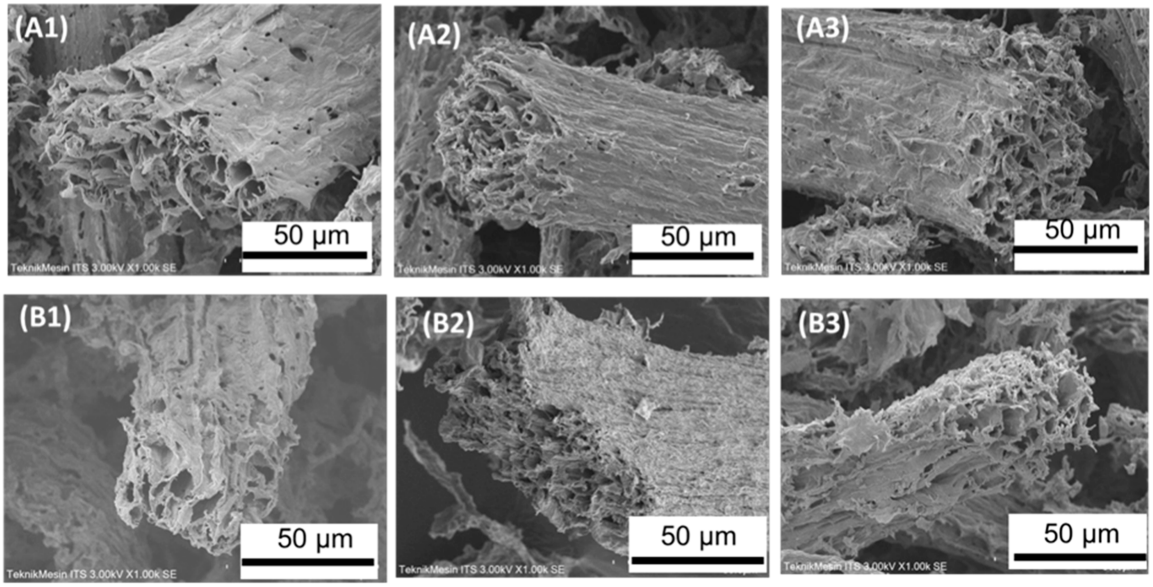


**Figure 2.** SEM images of coir fiber-based CaA pyrolyzed at various temperatures: (A1) 600; (A2) 700; and (A3) 800 °C and PEFB-based CaA pyrolyzed at various temperatures: (B1) 600; (B2) 700; and (B3) 800 °C.

**Table 1. Specific Surface Area of Carbon Aerogels Pyrolyzed at Various Temperatures and the Corresponding Cellulose Aerogel**

| raw materials | samples | pyrolysis temperature (°C) | surface area ($m^2\ g^{-1}$) | fiber diameter ($\mu$m) | internal pore size ($\mu$m) |
|---|---|---|---|---|---|
| CF | cellulose aerogel | | 86 | | |
| | carbon aerogel | 600 | 2510 | 61.21 ± 14.79 | 6.15 ± 1.84 |
| | carbon aerogel | 700 | 3603 | 55.67 ± 15.85 | 5.43 ± 1.41 |
| | carbon aerogel | 800 | 1951 | 48.88 ± 12.93 | 4.08 ± 0.96 |
| PEFB | cellulose aerogel | | 130 | | |
| | carbon aerogel | 600 | 3591 | 54.53 ± 21.11 | 5.47 ± 1.95 |
| | carbon aerogel | 700 | 4568 | 49.50 ± 19.93 | 4.72 ± 1.98 |
| | carbon aerogel | 800 | 2824 | 33.23 ± 20.80 | 3.36 ± 1.85 |

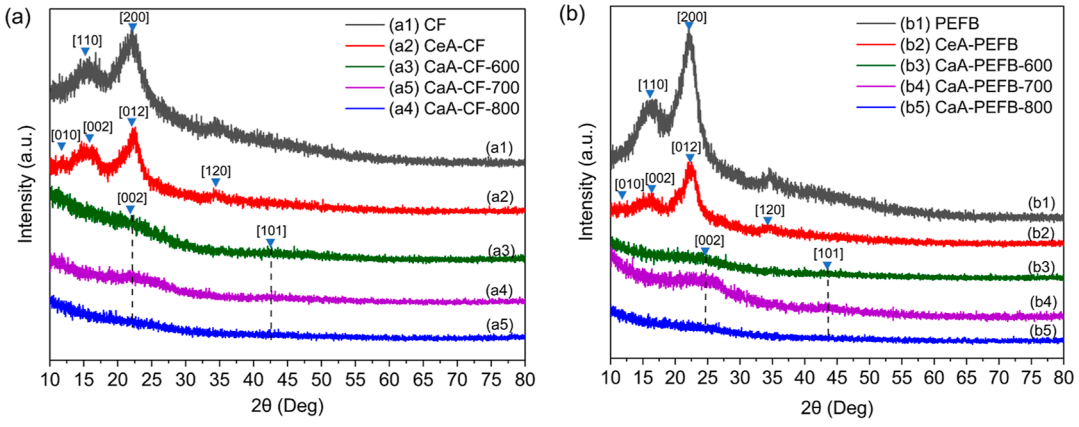


**Figure 3.** XRD patterns of aerogels derived from (a) CF: (a1) raw material, (a2) CeA, and (a3,a4) carbon aerogel pyrolyzed at 600 (a3), 700 (a4), and 800 °C (a5); (b) PEFB: (b1) raw material, (b2) CeA, and (b3,b4) carbon aerogel pyrolyzed at 600 (b3), 700 (b4), and 800 °C (b5).

NMP solvent in a weight ratio of 10:1:1 to obtain a homogeneous paste. The catalyst paste was then cast into a nickel foam. The Mg alloy AZ31B anode and carbon aerogel@nickel foam cathode with active areas of 1 $cm^2$ (1 cm × 1 cm) were assembled in a cell with a 3.5% NaCl electrolyte for the Mg−air full-cell testing. The full-cells were analyzed using a battery analyzer (model BST8-MA, MTI Corporation, USA).

## 3. RESULTS AND DISCUSSION

**3.1. Characteristics of N-Doped Carbon Aerogel.** The color of the cellulose aerogel derived from CF and PEFB changed from light brown to black after pyrolysis at 700 °C without changing their shape significantly (Figure S1). It is likely that the microstructure of cellulose aerogel could be maintained during the pyrolysis at high temperature. This is confirmed by the SEM images, as shown in Figure 1, showing


https://doi.org/10.1021/acsomega.3c09297
ACS Omega 2024, 9, 13994−14004

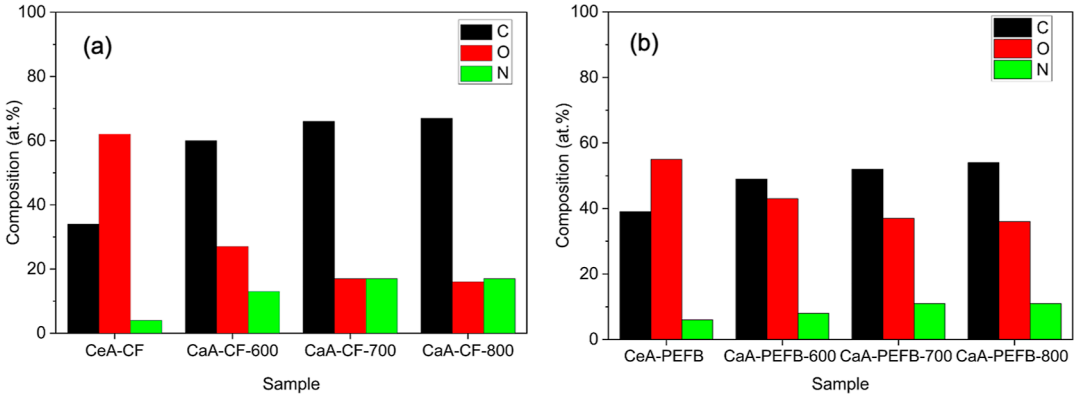


**Figure 4.** Compositions of the original CeA and CaA pyrolyzed at a temperature of 600, 700, and 800 °C: (a) CF and (b) PEFB.

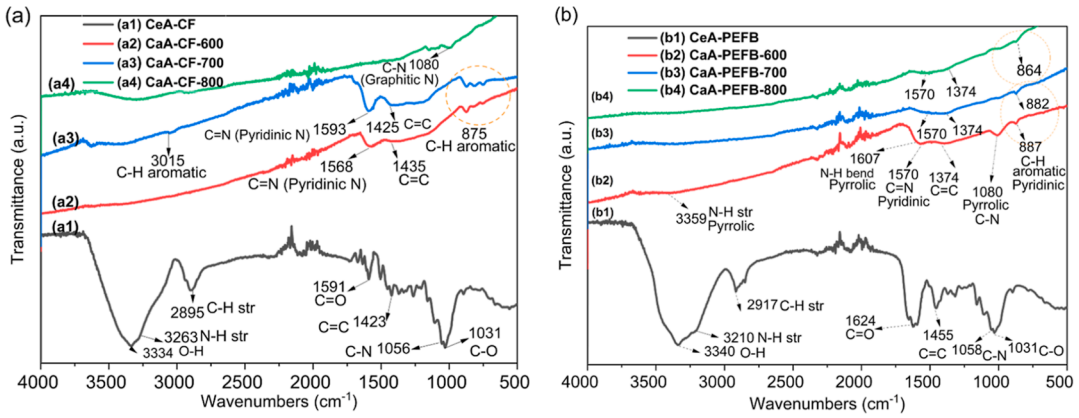


**Figure 5.** FTIR spectra of aerogels derived from (a) CF: (a1) CeA and (a2−a4) CaA pyrolyzed at 600 (a2), 700 (a3), and 800 °C (a4); (b) PEFB: (b1) CeA and (b2−b4) CaA pyrolyzed at 600 (b2), 700 (b3), and 800 °C (b4).

that the microstructure of cellulose aerogel (A1−C1) and the corresponding carbon aerogel (A2−C2) is similar. The cellulose aerogel and carbon aerogel have a porous structure composed of a three-dimensional network of interconnected fibers with a porosity of approximately 92.7% for cellulose aerogel and 96.2% for carbon aerogel. However, the size of fibers in carbon aerogel is smaller than that in cellulose aerogel. Observing the cross-sectional view of individual fibers, the internal pores of the fibers in carbon aerogels are larger than those of the corresponding cellulose aerogel.

Pyrolysis at different temperatures, i.e., 600 and 800 °C, yielded the same results for aerogels derived from both CF and PEFB. The shape and size of aerogels were relatively unchanged, and the microstructure of cellulose aerogels could be maintained after pyrolysis (Figure 2). The difference is on the fiber diameter and the internal pore fiber size of the resulting carbon aerogel, which for all cases tends to decrease with the increase of pyrolysis temperature. The fiber diameter of CF carbon aerogel pyrolyzed at 600, 700, and 800 °C was, respectively, 61.21, 55.67, and 48.88 $\mu$m, and the internal pore size was 6.15, 5.43, and 4.08 $\mu$m. For PEFB carbon aerogel, the fiber diameter for 600, 700, and 800 °C was, respectively, 54.53, 49.50, and 33.23 $\mu$m, and the internal pore size of the individual fiber was 5.47, 4.72, and 3.36 $\mu$m. The surface area of carbon aerogels was significantly increased from that of their corresponding cellulose aerogels after pyrolysis (Table 1). The surface areas of PEFB cellulose were higher than those of CF cellulose aerogel at the same pyrolysis temperature, with the highest-surface area obtained at a pyrolysis temperature of 700 °C for both materials. Observing the individual fibers of carbon aerogels shown in the SEM images of Figure 2, the internal pores of carbon aerogel pyrolyzed at 800 °C are larger than that of pyrolyzed at 700 °C. This may explain why the carbon aerogel pyrolyzed at 800 °C has smaller surface area.

Figure 3 shows the XRD patterns of cellulose aerogels and their corresponding carbon aerogels derived from CF and PEFB materials pyrolyzed at various temperatures. The diffraction patterns for both CF and PEFB have two characteristic peaks, a sharp peak at 22.1° (2 0 0) and a broad peak at 16.0° (1 1 0), which match the pattern of cellulose I.[40] The two peaks disappeared after their conversion into cellulose aerogels, replaced by four characteristic peaks at 11.7° (0 1 0), 16.6° (0 0 2), 22.2° (0 1 2), and 34.5° (1 2 0), which belong to cellulose III.[40] It is apparent that the dissolution and reprecipitation of cellulose in an aqueous $NH_3$−urea solvent changed the cellulose phase from cellulose I to cellulose III. After pyrolysis at either 600, 700, or 800 °C, the diffraction peaks changed to two broad peaks at 22.5° (0 0 2) and 42.5° (1 0 1), which can be indexed to amorphous carbon.[12] The broad diffraction peaks indicate that carbon experiences an exfoliation into few layers and long-range disorders.[12] The exfoliation may cause the doping of nitrogen into the carbon structure, resulting in C═N functional groups, as shown by the FTIR spectra, which will be discussed later. The (1 0 1) plane of carbon aerogel pyrolyzed at 700 °C appears to be less developed compared to the others, and the intensity of the (0 0 2) plane is the highest for both CF and PEFB carbon aerogels. These results suggest that the


https://doi.org/10.1021/acsomega.3c09297
ACS Omega 2024, 9, 13994−14004

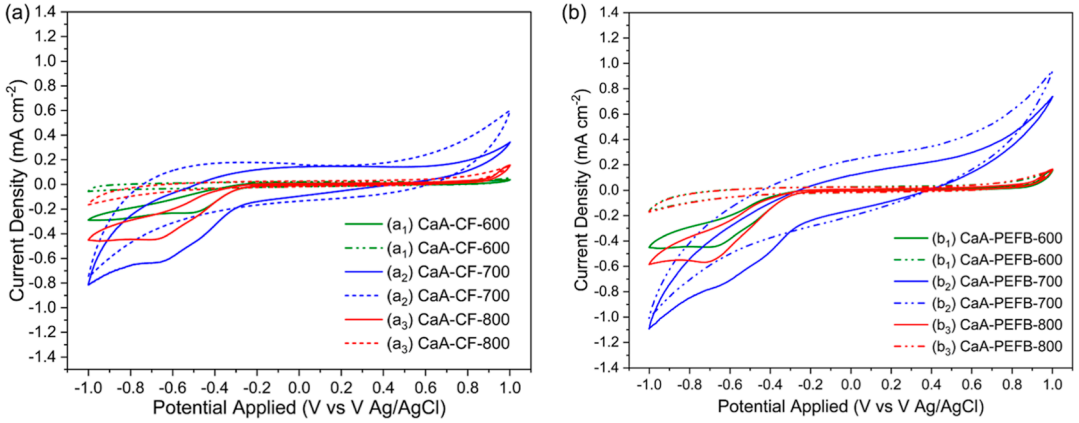


**Figure 6.** CV curves of N-doped aerogel in a 3.5% NaCl solution with a scan rate of 10 mV $s^{-1}$ from (a) carbon aerogel based on CF pyrolyzed at 600 ($a_1$), 700 ($a_2$), and 800 °C ($a_3$); (b) carbon aerogel based on PEFB pyrolyzed at 600 ($b_1$), 700 ($b_2$), and 800 °C ($b_3$). The solid-line curves were measured in an $O_2$-saturated solution, and dashed-line curves were measured in a $N_2$-saturated solution.

crystalline regularity is distorted, which may be due to the presence of C−N bonding, as shown by the FTIR spectra that will be discussed later.

Figure 4 shows the atomic compositions of carbon aerogels pyrolyzed at various temperatures and the starting materials of the corresponding cellulose aerogel derived from CF and PEFB with SEM−EDS. The carbon content of carbon aerogels increased after pyrolysis both for the aerogels derived from CF and PEFB, and it was higher by the increase of temperature. The high carbon content in the carbon aerogels made the color change from light brown to black. Moreover, the N content of carbon aerogels also tended to increase with the increase of pyrolysis temperature. Observing the FTIR spectra of cellulose aerogels and the resulting carbon aerogels after pyrolysis (Figure 5), some functional groups disappeared and new groups appeared. Most of the characteristic bands in the spectra that belong to cellulose disappeared, and new bands that belong to carbon and its related compounds appeared. The bands that belong to cellulose are at wavenumbers between 3334 and 3340 $cm^{-1}$ (O−H), 2895 $cm^{-1}$ (C−H stretch), between 1423 and 1455 $cm^{-1}$ (C═C bond), 1031 $cm^{-1}$ (C−O bond), between 1591 and 1624 $cm^{-1}$ (C═O bond), between 3210 and 3263 $cm^{-1}$ (N−H stretch), and between 1056 and 1058 $cm^{-1}$ (C−N bond).[41] The last three bands indicate the cross-link of cellulose molecules with urea molecules. The bands disappeared after pyrolysis because of the cellulose conversion into carbon, and they were replaced by new bands indicating the emergence of N-doped carbon. The nature of doping will be discussed in detail in the following.

The existence of N in the carbon aerogel has been evidenced by the characteristic bands in the FTIR spectra discussed earlier. At the pyrolysis temperature of 600 °C, the FTIR spectra of both CF and PEFB carbon aerogels show the presence of pyridinic N and pyrrolic N. The pyridinic N is indicated by the bands between 1568 and 1593 $cm^{-1}$ (C═N bond) along with the bands at 1425 $cm^{-1}$ (C═C bond) and at 880 $cm^{-1}$ (C−H aromatic bond), and the pyrrolic N is indicated by the bands at wavenumbers of 1080 $cm^{-1}$ (C−N bond), 1607 $cm^{-1}$ (N−H bond), and 3359 $cm^{-1}$ (N−H stretching).[42] The band indicating pyrrolic N at 1080 $cm^{-1}$ (C−N bond) disappeared when both the CF and PEFB cellulose aerogels were pyrolyzed at 700 °C. Instead, a new band indicating other aromatic C−H bond at a wavenumber of 3015 $cm^{-1}$ appeared. These signals indicate that pyrrole N has been replaced by pyridinic N in the carbon aerogels at a pyrolysis temperature of 700 °C for both CF and PEFB carbon aerogels. When the pyrolysis temperature was increased to 800 °C, the bands indicating pyridinic N weakened for both CF and PEFB carbon aerogels, and for the CF aerogel, a band at 1080 $cm^{-1}$ that can be attributed to graphitic N appeared. These results suggest that the nature of N doping on the carbon aerogels produced from CF and PEFB by direct pyrolysis is influenced by the pyrolysis temperature. Pyrrolic N tends to be formed at pyrolysis temperature of 600 °C, pyridinic N at 700 °C, and graphitic N at 800 °C (see Figure S3 for the chemical structure). It appears that the nature of N doping can simply be tuned by adjusting the pyrolysis temperature. It has been demonstrated in the published literature that the electrochemical active sites are generally derived from the vacancy defects of the $\pi$ system provided by pyrrolic N and pyridinic N.[23,43,44] Therefore, it could be expected that the N-doped carbon aerogels containing both types of N doping would have a high electrochemical reactivity.

**3.2. Electrocatalytic Activity toward ORR.** As a potential oxygen catalyst in the air−cathode of seawater batteries, the electrocatalytic activity of the prepared N-doped carbon aerogels was evaluated toward the ORR by CV and LSV measurements. Figure 6 shows the CV curves of the N-doped carbon aerogel pyrolyzed at various temperatures in $O_2$- and $N_2$-saturated 3.5% NaCl solutions at a scan rate of 10 mV $s^{-1}$. No peak can be observed in the CV curves of all N-doped carbon aerogels for a $N_2$-saturated 3.5% NaCl solution (Figure 6). The curves can provide a clean background for the $O_2$-saturated electrolyte. On the contrary, all N-doped carbon aerogels showed a higher cathodic peak in an $O_2$-saturated electrolyte. The peak potentials are at −0.67 V (vs Ag/AgCl) for all carbon aerogels except for CF carbon aerogel pyrolyzed at 600 °C. The peak potential for CF carbon aerogel pyrolyzed at 600 °C is approximately 0.5 V (vs Ag/AgCl). These indicate that the N-doped carbon aerogels have high electrocatalytic activity for the ORR. Another important criterion to evaluate ORR activity is onset potential.[45] N-doped CF and PEFB carbon aerogels pyrolyzed at 700 °C showed a larger shifted positively onset potential at −0.29 V (vs Ag/AgCl) and a higher current peak, implying that they have a higher electrocatalytic activity than the other samples. As discussed earlier, these samples have higher surface areas and contain


https://doi.org/10.1021/acsomega.3c09297
ACS Omega 2024, 9, 13994−14004

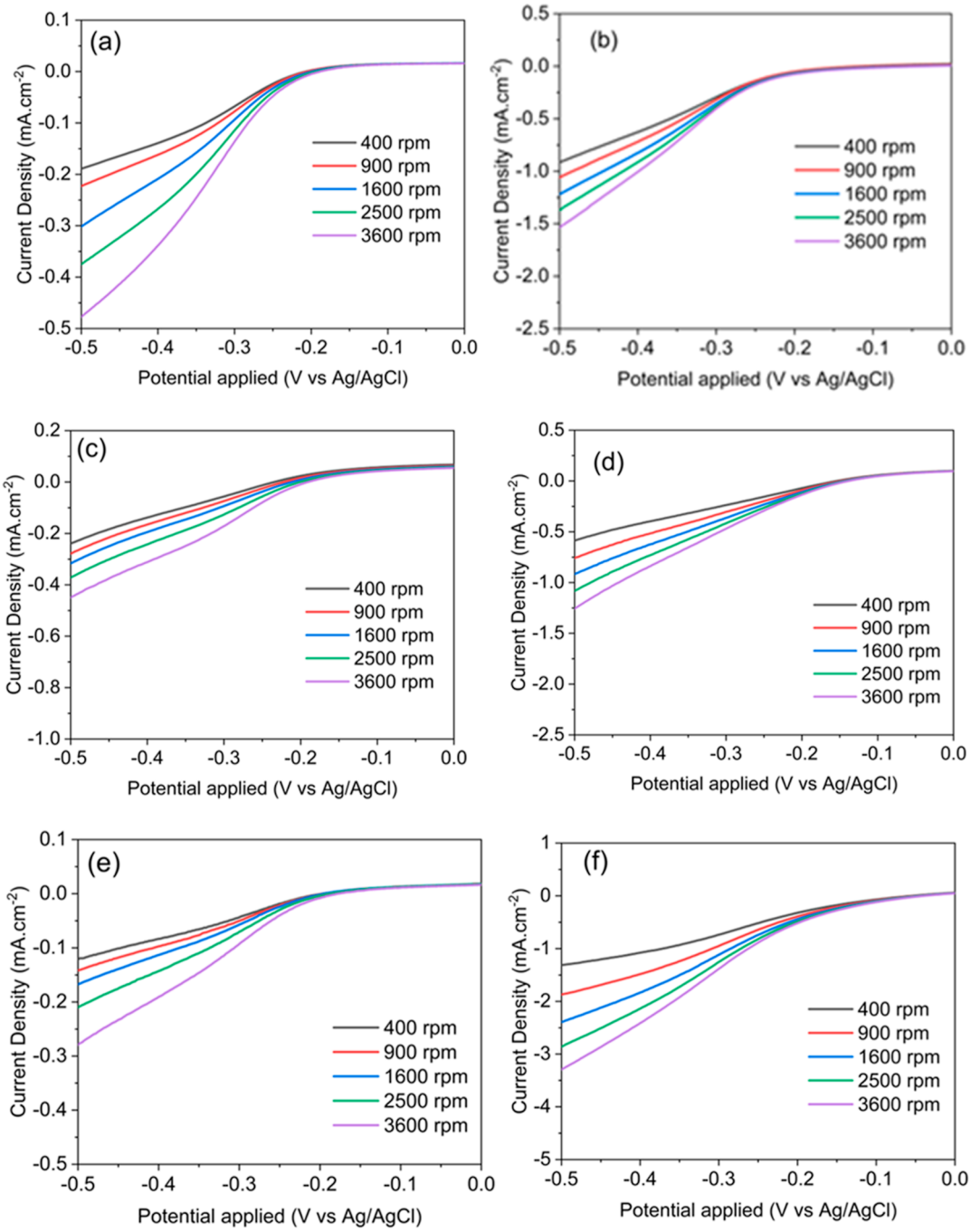


**Figure 7.** LSV curves of (a) CaA-CF-600, (b) CaA-PEFB-600, and (c) CaA-CF-700, (d) CaA-PEFB-700, (e) CaA-CF-800, and (f) CaA-PEFB-800 with a 3.5% NaCl electrolyte.

more pyridinic N that plays an important role in improving the ORR due to the vacancy defects. Therefore, they can provide more exposed active sites for the ORR than the other samples.

To further study the ORR activity of the prepared N-doped carbon aerogels, LSV measurements were performed in an $O_2$-saturated 3.5% NaCl solution using an RDE at a scan rate of 10 mV $s^{-1}$. Figure 7 shows the RDE voltammograms of CF and PEFB carbon aerogel samples prepared at different pyrolysis temperatures for the ORR at various rotation speeds. All N-doped carbon aerogel samples show an onset potential of approximately −0.2 V (vs Ag/AgCl). The kinetic current density and the number of electrons involved during ORR were further calculated by the K−L equation, and the results are shown in Table 2. The fitting lines of the K−L plots (Figure S4) are near parallel each other, indicating that the reactions are kinetically first-order with respect to the dissolved oxygen and have similar electron transfer numbers for the ORR at different potentials.[46] The kinetic current density of both CF and PEFB carbon aerogel samples pyrolyzed at 700 °C showed the maximum value, namely, 0.65 mA $cm^{-2}$ for CE and 0.50 mA $cm^{-2}$ for PEFB. As discussed earlier, the carbon aerogel samples pyrolyzed at 700 °C contain more pyridinic N than the other samples, and thus, we speculate that the kinetic current density increased positively with the amount of pyridinic N. The calculated electron transfer numbers ($n$) for


https://doi.org/10.1021/acsomega.3c09297
ACS Omega 2024, 9, 13994−14004

**Table 2. Average Number of Electron Displacement ($n$) and Kinetic Current Density ($i_k$) of the Carbon Aerogels Are Based on the Koutecký–Levich Equation**

| sources of cellulose | pyrolysis temperature (°C) | $n$ (−) | $i_k$ (mA cm$^{-2}$) |
|---|---|---|---|
| CF | 600 | 3.36 | 0.61 |
| | 700 | 3.54 | 0.65 |
| | 800 | 2.20 | 0.26 |
| PEFB | 600 | 3.01 | 0.11 |
| | 700 | 3.96 | 0.50 |
| | 800 | 2.86 | 0.19 |

both CF and PEFB carbon aerogels pyrolyzed at 600 and 700 °C approach 4 following the reaction[47]

$$O_2 + 2H_2O + 4e^- \rightarrow 4OH^- \quad (4)$$

For both CF and PEFB carbon aerogels pyrolyzed at 800 °C, the calculated electron transfer numbers approach 2 following the reactions[47]

$$O_2 + H_2O + 2e^- \rightarrow HO_2^- + OH^- \quad (5)$$

$$H_2O + HO_2^- + 2e^- \rightarrow 3OH^- \quad (6)$$

Again, the electron transfer numbers of carbon aerogel samples pyrolyzed at 700 °C approach 4, i.e., the ORR follows the four-electron pathway, which quantitatively implies a more electrochemically stable process.[47] These LSV results are consistent with the results of CV analysis, indicating that samples with the highest proportion of pyridinic N could improve an ORR by changing the ORR mechanism to direct the four-electron pathway to water. Although both CF and PEFB carbon aerogel samples pyrolyzed at 800 °C have similar proportion of N (Figure 4), their ORR performance is less enhanced than those pyrolyzed at 700 °C. The type of N doping on these carbon aerogels is dominated by graphitic N, not pyridinic N, which does not have many vacancy defects that serve as the electrochemical active sites.

In general, pyridinic N is the main active site for the $O_2$ adsorption reduction that facilitates ORR by creating Lewis base to adsorb oxygen molecule at the carbon atom next to the pyridinic N followed by protonation of the adsorbed $O_2$.[20] As discussed earlier, the ORR of both CF and PEFB carbon aerogels pyrolyzed at 700 °C followed the four-electron pathway due to the higher proportion of pyridinic N. In the four-electron pathway, the other two protons attach to the oxygen atoms, which break the O–OH bond up to form OH species (Figure S5). The adsorbed OH species then reacts with the additional proton to form $H_2O$. The presence of carbon atoms next to pyridinic N with Lewis basicity plays an important role in providing active sites for the adsorption of oxygen molecules as the initial step of the ORR.

Although not as active as pyridinic N, pyrrolic N and graphitic N can also serve as active sites for the ORR following a two-electron pathway. In this case, pyrrolic N and graphitic N facilitate ORR by creating Lewis base as the active sites for the adsorption of oxygen molecule as the initial step of the ORR followed by protonation of the adsorbed oxygen to form O–OH (see Figures S6 and S7). Then, $H_2O_2$ is formed by the reaction of the adsorbed O–OH species with another proton, followed by readsorption of $H_2O_2$ and its reduction by two protons to generate $H_2O$.[20]

**3.3. Performance of Mg–Air Battery Using the Pyridinic-N Carbon Aerogels.** To demonstrate the practical performance of the N-doped carbon aerogels as an ORR catalyst in seawater batteries, we assembled Mg–air batteries using commercial Mg alloy as the anode and N-doped carbon aerogels (CF and PEFB pyrolyzed at 700 °C) as the cathode (Figure S8). The electrolyte was a 3.5% NaCl solution. As shown in Figure 8, using a galvanostatic discharge current of 1 mA cm$^{-2}$, the Mg–air batteries using a 3.5% NaCl electrolyte showed a relatively constant voltage of approximately 1.1 V for both CF and PEFB carbon aerogels for relatively long time. The discharge voltage dropped sharply after the discharge tests of 15.5 and 18.9 h for CF- and PEFB-carbon aerogels, respectively. The Mg–air batteries using the CF- and PEFB-N-doped carbon aerogels delivered a high discharge capacity of, respectively, 411.64 and 492.64 mA h g$^{-1}$, corresponding to an energy density of 464.23 and 529.49 mW h g$^{-1}$. These high-power densities are considered to be successfully rapid oxygen transport on the catalyst layer, which plays an important role as a water-flooding three-phase boundary. The sudden drop in voltage after the long discharge time might not be caused by the exhausted catalyst layer but might be caused by the formation of a passive layer at the Mg anode. We observed the formation of white precipitate, more likely $Mg(OH)_2$, during the discharge process, leading to covering up the surface of Mg

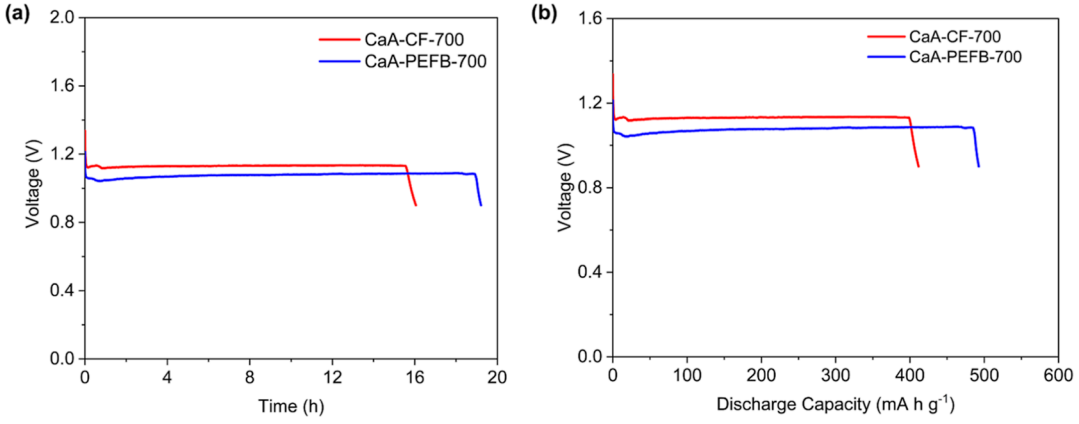


**Figure 8.** (a) Discharge voltage and (b) discharge capacity of seawater battery were tested for the discharge process at a constant current density of 1 mA cm$^{-2}$ with N-doped carbon aerogel of CaA-CF-700 and CaA-PEFB-700 as the air cathode, magnesium alloy as the anode, and electrolyte of NaCl 3.5%.



https://doi.org/10.1021/acsomega.3c09297
ACS Omega 2024, 9, 13994−14004

anode and electrically separating the anode from the electrolyte.

## 4. CONCLUSIONS

We have demonstrated that the nature of N doping on carbon aerogels derived from biomass, i.e., CF and PEFB, can be tuned simply by adjusting the pyrolysis temperature of the prepared cellulose aerogels. The type of N doping is dominated by pyrrolic N at pyrolysis temperature of 600 °C, changes to pyridinic N at 700 °C, and finally to graphitic N at 800 °C. Electrochemical tests show that pyridinic N can serve as active sites to facilitate the ORR and has better performance as the electrocatalyst for the ORR than pyrrolic N and graphitic N. The ORR using pyridinic N follows the four-electron pathway, which quantitatively implies a more electrochemically stable process. Another type of N-doped carbon is required in providing active sites for the adsorption of oxygen molecules as the initial step of the ORR. Assembling the pyridinic N carbon aerogels into the Mg−air battery with a 3.5% NaCl electrolyte gives a cell voltage of approximately 1.1 V. The battery cell can deliver a high discharge capacity of 411.64 mA h $g^{-1}$ for CF and 492.64 mA h $g^{-1}$ for PEFB corresponding to an energy density of 464.23 and 529.49 mW h $g^{-1}$, respectively. The biomass-based N-doped carbon aerogels may be also used as the matrix for its counterpart oxygen evolution reaction to fabricate a bifunctional electrocatalyst for rechargeable seawater batteries.

## ■ ASSOCIATED CONTENT

### Supporting Information

The Supporting Information is available free of charge at https://pubs.acs.org/doi/10.1021/acsomega.3c09297.

Additional experimental data including photographs of cellulose and carbon aerogels, $N_2$ adsorption isotherm curves of carbon aerogels, FTIR spectra, K−L plots, 4- and 2-electron pathways of ORR at pyridinic N carbon aerogels, 2-electron pathway of ORR at pyrrolic N and graphitic N carbon aerogels, and seawater battery for the discharge process with N-doped carbon aerogel as the air cathode (PDF)

## ■ AUTHOR INFORMATION


### Corresponding Author

**Heru Setyawan** − *Department of Chemical Engineering, Sepuluh Nopember Institute of Technology, Surabaya 60111, Indonesia;* orcid.org/0000-0002-2158-6819; Phone: +62 31 5946240; Email: sheru@chem-eng.its.ac.id; Fax: +62 31 5999282

### Authors

**Susanto Susanto** − *Department of Chemical Engineering, Sepuluh Nopember Institute of Technology, Surabaya 60111, Indonesia;* Present Address: On leave from Politeknik Negeri Malang, Jl. Soekarno-Hatta No. 9, Malang 65141, Indonesia. Email: susanto.s@polinema.ac.id; orcid.org/0000-0003-0862-5622

**Tantular Nurtono** − *Department of Chemical Engineering, Sepuluh Nopember Institute of Technology, Surabaya 60111, Indonesia*

**Widiyastuti Widiyastuti** − *Department of Chemical Engineering, Sepuluh Nopember Institute of Technology, Surabaya 60111, Indonesia;* orcid.org/0000-0002-2805-2836

**Min-Hsin Yeh** − *Department of Chemical Engineering, National Taiwan University of Science and Technology, Taipei 10607, Taiwan;* orcid.org/0000-0002-6150-4750

Complete contact information is available at: https://pubs.acs.org/10.1021/acsomega.3c09297


### Notes

The authors declare no competing financial interest.

## ■ ACKNOWLEDGMENTS

This work has been partially funded by PT PERTAMINA (Persero) and the Ministry of Education, Culture, Research and Technology of the Republic of Indonesia through Kedaireka Matching Fund Program (contract nos. 1183/PKS/ITS/2023 and 114/E1/HK.02.02/2023). One of the authors (S.S.) would like to thank the Centre for Higher Education Funding (BPPT-PUSLAPDIK) of the Ministry of Education, Culture, Research and Technology of Indonesia for the BPI Doctoral scholarship. We thank Ulfiana Ihda Afifa, Taris Farizan Rochman, and Muhammad Rivaldy Kamandanu for their assistance with the experiments.

## ■ REFERENCES


(1) Li, M.; Lu, J.; Chen, Z.; Amine, K. 30 Years of Lithium-Ion Batteries. *Adv. Mater.* **2018**, *30* (33), 1800561.

(2) Liu, Q.; Pan, Z.; Wang, E.; An, L.; Sun, G. Aqueous Metal-Air Batteries: Fundamentals and Applications. *Energy Storage Mater.* **2020**, *27*, 478−505.

(3) Clark, S.; Mainar, A. R.; Iruin, E.; Colmenares, L. C.; Blázquez, J. A.; Tolchard, J. R.; Jusys, Z.; Horstmann, B. Designing Aqueous Organic Electrolytes for Zinc-Air Batteries: Method, Simulation, and Validation. *Adv. Energy Mater.* **2020**, *10* (10), 1903470.

(4) Tarigan, A. M.; Aulia, S.; Rinawati, M.; Chang, L.-Y.; Cheng, Y.-S.; Chang, C.-C.; Huang, W.-H.; Chen, J.-L.; Setyawan, H.; Yeh, M.-H. Tandem Surface Engineering of Graphene Quantum Dot-Assisted Fluorinated NiFe Prussian Blue Analogue for Electrocatalytic Oxygen Evolution Reaction. *Chem. Eng. J.* **2023**, *476*, 146754.

(5) Hwang, S. M.; Park, J. S.; Kim, Y.; Go, W.; Han, J.; Kim, Y.; Kim, Y. Rechargeable Seawater Batteries—From Concept to Applications. *Adv. Mater.* **2019**, *31* (20), 1804936.

(6) Shinohara, M.; Araki, E.; Mochizuki, M.; Kanazawa, T.; Suyehiro, K. Practical Application of a Sea-Water Battery in Deep-Sea Basin and Its Performance. *J. Power Sources* **2009**, *187* (1), 253−260.

(7) Ryu, J. H.; Park, J.; Park, J.; Mun, J.; Im, E.; Lee, H.; Hong, S. Y.; An, K.; Lee, G.; Kim, Y.; Jo, P. S.; Kang, S. J. Carbothermal Shock-Induced Bifunctional Pt-Co Alloy Electrocatalysts for High-Performance Seawater Batteries. *Energy Storage Mater.* **2022**, *45*, 281−290.

(8) Wang, L.; Snihirova, D.; Deng, M.; Vaghefinazari, B.; Xu, W.; Höche, D.; Lamaka, S. V.; Zheludkevich, M. L. Sustainable Aqueous Metal-Air Batteries: An Insight into Electrolyte System. *Energy Storage Mater.* **2022**, *52*, 573−597.

(9) Li, Q.; Xiong, W.; Yu, S.; Liu, Y.; Li, J.; Liu, L.; Bi, X.; Zhu, G.; Liu, E.; Zhao, Y.; Wang, B. Effect of Gd Content on the Discharge and Electrochemical Behaviors of the Magnesium Alloy AZ31 as an Anode for Mg-Air Battery. *J. Mater. Sci.* **2021**, *56* (22), 12789−12802.

(10) Yu, J.; Li, B.-Q.; Zhao, C.-X.; Zhang, Q. Seawater Electrolyte-Based Metal-Air Batteries: From Strategies to Applications. *Energy Environ. Sci.* **2020**, *13* (10), 3253−3268.

(11) Yanchun, Z.; Guangsheng, H.; Cheng, Z.; Lin, C.; Ting-zhuang, H.; Fusheng, P. Effect of Texture on the Performance of Mg-Air Battery Based on Rolled Mg-3Al-1Zn Alloy Sheet. *Rare Met. Mater. Eng.* **2018**, *47* (4), 1064−1068.

(12) Fauziyah, M.; Widiyastuti, W.; Setyawan, H. Nitrogen-Doped Carbon Aerogels Prepared by Direct Pyrolysis of Cellulose Aerogels Derived from Coir Fibers Using an Ammonia-Urea System and Their Electrocatalytic Performance toward the Oxygen Reduction Reaction. *Ind. Eng. Chem. Res.* **2020**, *59* (49), 21371−21382.
(13) Yang, C.; Liu, Z. 7-Bifunctional OER-ORR Electrodes for Metal-Air Batteries. In *Metal Oxide-Based Nanostructured Electrocatalysts for Fuel Cells, Electrolyzers, and Metal-air Batteries*; Napporn, T. W., Holade, Y., Eds.; Elsevier, 2021; pp 139−186.
(14) Li, Y.; Guo, S. Noble Metal-Based 1D and 2D Electrocatalytic Nanomaterials: Recent Progress, Challenges and Perspectives. *Nano Today* **2019**, *28*, 100774.
(15) Liu, M.; Xiao, X.; Li, Q.; Luo, L.; Ding, M.; Zhang, B.; Li, Y.; Zou, J.; Jiang, B. Recent Progress of Electrocatalysts for Oxygen Reduction in Fuel Cells. *J. Colloid Interface Sci.* **2022**, *607*, 791−815.
(16) Deng, J.; Fang, S.; Fang, Y.; Hao, Q.; Wang, L.; Hu, Y. H. Multiple Roles of Graphene in Electrocatalysts for Metal-Air Batteries. *Catal. Today* **2023**, *409*, 2−22.
(17) Zhuang, S.; Lee, E. S.; Lei, L.; Nunna, B. B.; Kuang, L.; Zhang, W. Synthesis of Nitrogen-Doped Graphene Catalyst by High-Energy Wet Ball Milling for Electrochemical Systems. *Int. J. Energy Res.* **2016**, *40* (15), 2136−2149.
(18) Lv, Q.; Si, W.; He, J.; Sun, L.; Zhang, C.; Wang, N.; Yang, Z.; Li, X.; Wang, X.; Deng, W.; Long, Y.; Huang, C.; Li, Y. Selectively Nitrogen-Doped Carbon Materials as Superior Metal-Free Catalysts for Oxygen Reduction. *Nat. Commun.* **2018**, *9* (1), 3376.
(19) Liang, H. W.; Zhuang, X.; Brüller, S.; Feng, X.; Müllen, K. Hierarchically Porous Carbons with Optimized Nitrogen Doping as Highly Active Electrocatalysts for Oxygen Reduction. *Nat. Commun.* **2014**, *5*, 4973.
(20) Guo, D.; Shibuya, R.; Akiba, C.; Saji, S.; Kondo, T.; Nakamura, J. Active Sites of Nitrogen-Doped Carbon Materials for Oxygen Reduction Reaction Clarified Using Model Catalysts. *Science* **2016**, *351* (6271), 361−365.
(21) Sakaushi, K.; Lyalin, A.; Tominaka, S.; Taketsugu, T.; Uosaki, K. Two-Dimensional Corrugated Porous Carbon-Nitrogen-Framework/Metal Heterojunction for Efficient Multielectron Transfer Processes with Controlled Kinetics. *ACS Nano* **2017**, *11* (2), 1770−1779.
(22) Fukushima, T.; Drisdell, W.; Yano, J.; Surendranath, Y. Graphite-Conjugated Pyrazines as Molecularly Tunable Heterogeneous Electrocatalysts. *J. Am. Chem. Soc.* **2015**, *137* (34), 10926−10929.
(23) Bai, X.; Shi, Y.; Guo, J.; Gao, L.; Wang, K.; Du, Y.; Ma, T. Catalytic Activities Enhanced by Abundant Structural Defects and Balanced N Distribution of N-Doped Graphene in Oxygen Reduction Reaction. *J. Power Sources* **2016**, *306*, 85−91.
(24) Meng, F.; Li, L.; Wu, Z.; Zhong, H.; Li, J.; Yan, J. Facile Preparation of N-Doped Carbon Nanofiber Aerogels from Bacterial Cellulose as an Efficient Oxygen Reduction Reaction Electrocatalyst. *Chin. J. Catal.* **2014**, *35* (6), 877−883.
(25) Yu, M.; Han, Y.; Li, J.; Wang, L. One-Step Synthesis of Sodium Carboxymethyl Cellulose-Derived Carbon Aerogel/Nickel Oxide Composites for Energy Storage. *Chem. Eng. J.* **2017**, *324*, 287−295.
(26) Liang, H.; Wu, Z.; Chen, L.; Li, C.; Yu, S. H. Bacterial Cellulose Derived Nitrogen-Doped Carbon Nano Fiber Aerogel: An Efficient Metal-Free Oxygen Reduction Electrocatalyst for Zinc-Air Battery. *Nano Energy* **2015**, *11*, 366−376.
(27) Alwin, S.; Sahaya Shajan, X. Aerogels: Promising Nanostructured Materials for Energy Conversion and Storage Applications. *Mater. Renew. Sustain. Energy* **2020**, *9* (2), 7.
(28) Sridhar, V.; Lee, I.; Chun, H.-H.; Park, H. Microwave Synthesis of Nitrogen-Doped Carbon Nanotubes Anchored on Graphene Substrates. *Carbon* **2015**, *87*, 186−192.
(29) Wang, X.; Li, X.; Zhang, L.; Yoon, Y.; Weber, P. K.; Wang, H.; Guo, J.; Dai, H. N-Doping of Graphene Through Electrothermal Reactions with Ammonia. *Science* **2009**, *324* (5928), 768−771.
(30) Fauziyah, M.; Widiyastuti, W.; Setyawan, H. Sulfonated Carbon Aerogel Derived from Coir Fiber as High Performance Solid Acid Catalyst for Esterification. *Adv. Powder Technol.* **2020**, *31* (4), 1412−1419.
(31) Mainali, K.; Mood, S. H.; Pelaez-Samaniego, M. R.; Sierra-Jimenez, V.; Garcia-Perez, M. Production and Applications of N-Doped Carbons from Bioresources: A Review. *Catal. Today* **2023**, *423*, 114248.
(32) Debono, O.; Villot, A. Nitrogen Products and Reaction Pathway of Nitrogen Compounds during the Pyrolysis of Various Organic Wastes. *J. Anal. Appl. Pyrolysis* **2015**, *114*, 222−234.
(33) Chen, W.; Yang, H.; Chen, Y.; Xia, M.; Chen, X.; Chen, H. Transformation of Nitrogen and Evolution of N-Containing Species during Algae Pyrolysis. *Environ. Sci. Technol.* **2017**, *51* (11), 6570−6579.
(34) Zhou, H.; Zhang, J.; Amiinu, I. S.; Zhang, C.; Liu, X.; Tu, W.; Pan, M.; Mu, S. Transforming Waste Biomass with an Intrinsically Porous Network Structure into Porous Nitrogen-Doped Graphene for Highly Efficient Oxygen Reduction. *Phys. Chem. Chem. Phys.* **2016**, *18* (15), 10392−10399.
(35) Pan, F.; Cao, Z.; Zhao, Q.; Liang, H.; Zhang, J. Nitrogen-Doped Porous Carbon Nanosheets Made from Biomass as Highly Active Electrocatalyst for Oxygen Reduction Reaction. *J. Power Sources* **2014**, *272*, 8−15.
(36) Sukmawan, R.; Kusmono; Rahmanta, A. P.; Saputri, L. H. The Effect of Repeated Alkali Pretreatments on the Morphological Characteristics of Cellulose from Oil Palm Empty Fruit Bunch Fiber-Reinforced Epoxy Adhesive Composite. *Int. J. Adhes. Adhes.* **2022**, *114*, 103095.
(37) Setyawan, H.; Fauziyah, M.; Tomo, H. S. S.; Widiyastuti, W.; Nurtono, T. Fabrication of Hydrophobic Cellulose Aerogels from Renewable Biomass Coir Fibers for Oil Spillage Clean-Up. *J. Polym. Environ.* **2022**, *30*, 5228−5238.
(38) Gojković, S.; Zečević, S.; Obradović, M.; DražIć, D. Oxygen Reduction on a Duplex Stainless Steel. *Corros. Sci.* **1998**, *40* (6), 849−860.
(39) van Stroe, A. J.; Janssen, L. J. J. Determination of the Diffusion Coefficient of Oxygen in Sodium Chloride Solutions with a Transient Pulse Technique. *Anal. Chim. Acta* **1993**, *279* (2), 213−219.
(40) French, A. D. Idealized Powder Diffraction Patterns for Cellulose Polymorphs. *Cellulose* **2014**, *21* (2), 885−896.
(41) Fauziyah, M.; Widiyastuti, W.; Balgis, R.; Setyawan, H. Production of Cellulose Aerogels from Coir Fibers via an Alkali-Urea Method for Sorption Applications. *Cellulose* **2019**, *26* (18), 9583−9598.
(42) Zhang, Y.; Wang, F.; Zhu, H.; Zhou, L.; Zheng, X.; Li, X.; Chen, Z.; Wang, Y.; Zhang, D.; Pan, D. Preparation of Nitrogen-Doped Biomass-Derived Carbon Nanofibers/Graphene Aerogel as a Binder-Free Electrode for High Performance Supercapacitors. *Appl. Surf. Sci.* **2017**, *426*, 99−106.
(43) Zhao, D.; Sun, K.; Cheong, W.-C.; Zheng, L.; Zhang, C.; Liu, S.; Cao, X.; Wu, K.; Pan, Y.; Zhuang, Z.; Hu, B.; Wang, D.; Peng, Q.; Chen, C.; Li, Y. Synergistically Interactive Pyridinic-N-MoP Sites: Identified Active Centers for Enhanced Hydrogen Evolution in Alkaline Solution. *Angew. Chem., Int. Ed.* **2020**, *59* (23), 8982−8990.
(44) Zhang, Q.; Cao, Y.; Yan, Y.; Yuan, B.; Zheng, H.; Gu, Y.; Zhong, X.; Wang, J. Synergetic Effect of Pyrrolic-N and Doped Boron in Mesoporous Carbon for Electrocatalytic Ozone Production. *J. Mater. Chem. A* **2020**, *8* (5), 2336−2342.
(45) Razmjooei, F.; Singh, K. P.; Song, M. Y.; Yu, J.-S. Enhanced Electrocatalytic Activity Due to Additional Phosphorous Doping in Nitrogen and Sulfur-Doped Graphene: A Comprehensive Study. *Carbon* **2014**, *78*, 257−267.
(46) Wang, G.; Xu, X.; Kou, X.; Liu, X.; Dong, X.; Ma, H.; Wang, D. N-Doping of Graphene Aerogel as a Multifunctional Air Cathode for Microbial Fuel Cells. *ACS Appl. Mater. Interfaces* **2021**, *13* (43), 51312−51320.
(47) Kim, H. W.; Bukas, V. J.; Park, H.; Park, S.; Diederichsen, K. M.; Lim, J.; Cho, Y. H.; Kim, J.; Kim, W.; Han, T. H.; Voss, J.; Luntz, A. C.; McCloskey, B. D. Mechanisms of Two-Electron and Four-


https://doi.org/10.1021/acsomega.3c09297
*ACS Omega* 2024, 9, 13994−14004

Electron Electrochemical Oxygen Reduction Reactions at Nitrogen-Doped Reduced Graphene Oxide. *ACS Catal.* **2020**, *10* (1), 852−863.



https://doi.org/10.1021/acsomega.3c09297
*ACS Omega* 2024, 9, 13994−14004